AD-A125 755 SPECTRAL DIAGNOSIS OF PLASMAS WITH 2-DIMENSIONAL NON-UNIFORMITIES(U) NAVAL RESEARCH LAB WASHINGTON DC D DUSTON ET AL. 18 MAR 83 NRL-MR-5038 1/1

UNCLASSIFIED F/G 7/4 NL

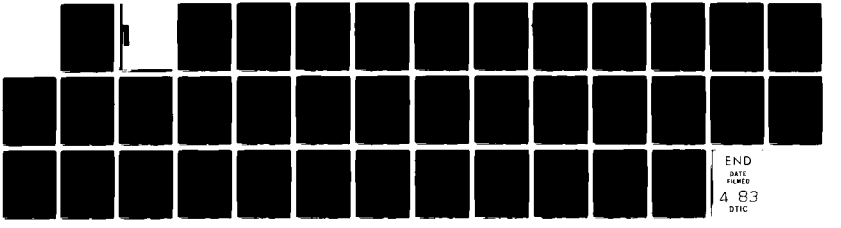

END
DATE FILMED
4 83
DTIC

M-2

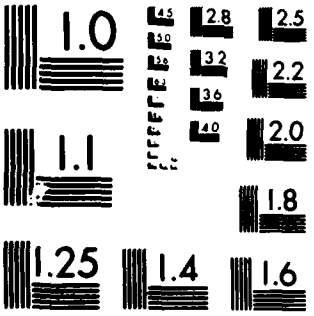

SECURITY CLASSIFICATION OF THIS PAGE (When Data Entered)

REPORT DOCUMENTATION PAGE		READ INSTRUCTIONS BEFORE COMPLETING FORM
1. REPORT NUMBER NRL Memorandum Report 5038	2. GOVT ACCESSION NO.	3. RECIPIENT'S CATALOG NUMBER
4. TITLE (and Subtitle) SPECTRAL DIAGNOSIS OF PLASMAS WITH 2-DIMENSIONAL NON-UNIFORMITIES		5. TYPE OF REPORT & PERIOD COVERED Interim report on a continuing NRL problem. 6. PERFORMING ORG. REPORT NUMBER
7. AUTHOR(s) D. Duston and J. Davis		8. CONTRACT OR GRANT NUMBER(s)
9. PERFORMING ORGANIZATION NAME AND ADDRESS Naval Research Laboratory Washington, D.C. 20375		10. PROGRAM ELEMENT, PROJECT, TASK AREA & WORK UNIT NUMBERS 61715H; 00006; 47-0857-0-3
11. CONTROLLING OFFICE NAME AND ADDRESS Defense Nuclear Agency Washington, D.C. 20305		12. REPORT DATE March 18, 1983 13. NUMBER OF PAGES 37
14. MONITORING AGENCY NAME & ADDRESS(if different from Controlling Office)		15. SECURITY CLASS. (of this report) UNCLASSIFIED 15a. DECLASSIFICATION/DOWNGRADING SCHEDULE

16. DISTRIBUTION STATEMENT (of this Report)

Approved for public release; distribution unlimited.

17. DISTRIBUTION STATEMENT (of the abstract entered in Block 20, if different from Report)

18. SUPPLEMENTARY NOTES

This research was sponsored by the Defense Nuclear Agency under Subtask T99QAXLA, work unit 00037 and work unit title "Source Development Theory," MIPR No. 82-519.

19. KEY WORDS (Continue on reverse side if necessary and identify by block number)

X-ray diagnostics
Laser-plasma
Radiation transport
Atomic processes
Plasma ionization

20. ABSTRACT (Continue on reverse side if necessary and identify by block number)

A series of investigations concerning new techniques in x-ray spectroscopy of dense plasmas is reported on. Included are two improvements in the ionization-radiation model used to diagnose experimental spectral data from dense laboratory plasma: (1) a detailed model for dielectronic satellite line emission in dense plasmas, (2) an integration scheme for the time-dependent atomic rate equations used to characterize collisional-radiative plasmas at highly non-equilibrium conditions. The model is then used to study 2-dimensional radiation phenomena in laser-heated plasmas. First, we investigate the effects of neglecting axial photon transport in the plasma blowoff on tracer-dot spectroscopy and subsequent

(Continues)

DD FORM 1 JAN 73 1473 EDITION OF 1 NOV 65 IS OBSOLETE
S/N 0102-014-6601

SECURITY CLASSIFICATION OF THIS PAGE (When Data Entered)

20. ABSTRACT (Continued)

temperature and density determinations. We find that the measured density may be as much as a factor of 2 in error when these effects are neglected, but measured temperatures are fortuitously correct to about 10%. Second, lateral inhomogeneities in plasma parameters are studied as they affect the K-shell X-ray spectrum emitted between the critical and ablation surface. A method is proposed to detect these non-uniformities via the techniques of tracer-dot spectroscopy.

CONTENTS

SPECTRAL DIAGNOSIS OF PLASMAS WITH 2-DIMENSIONAL NON-UNIFORMITIES

I. INTRODUCTION

Recent advances in experimental spectroscopy of dense laboratory plasmas have aroused renewed interest in radiation diagnostics as a means to determine plasma parameters. The purpose of this report is to document preliminary work, first presented at the 1982 Plasma Physics Divisional APS Meeting[1], regarding new diagnostic techniques in theoretical plasma spectroscopy, in particular, as they impact studies of laser-produced plasmas. While the results presented here are only preliminary, the trends are believed to be substantial, and more thorough documentation of a number of the topics discussed here is expected to emerge from more comprehensive follow-up studies.

The main thrust of this study is to investigate 2-dimensional plasma non-uniformities and the way in which they affect the x-ray spectrum emitted by the plasma. Our motivation in this work is twofold: first, we attempt to clarify some of the assumptions made in early tracer-dot implant analysis done at NRL; second, we seek to determine if fluid instabilities (e.g., Rayleigh-Taylor) can be detected and measured using the refined techniques of x-ray spectral analysis. In this report we discuss three important phenomena and how they effect the plasma radiation signature:

(1) time-dependent effects on ionization modeling, particularly in the blow-off of laser-plasmas where recombination (or ionization) time scales can be extremely long

(2) Two-dimensional radiation transport effects on the x-ray spectrum in experimental configurations where photon re-absorption is significant in directions both parallel and perpendicular to the spectrometer line-of-sight

(3) inhomogeneities in plasma temperature and density along the lateral direction, perpendicular to the laser beam, caused by plasma instabilities, non-uniformities in the laser profile, etc.

Before presenting the results of these studies, a brief description of the theoretical model follows.

Manuscript approved January 10, 1983.

II. Ionization-Radiation Model

To solve for the ionization state and radiation environment of the dense plasma we employ a collisional-radiative (CR) model which solves a set of atomic rate equations for the ion level population distribution. In addition, a fully-coupled radiation transport scheme employing probability-of-escape photon transport concepts[2] is used to calculate the radiation emission as well as the radiation trapping effects on the level populations. The model is one-dimensional and includes no plasma energetics or motional effects, relying on externally-generated plasma temperatures and densities for input. Details of this model are well-documented in a series of published papers[3]; further elaboration will not provide additional insight and therefore will be omitted.

The radiation patterns to be studies here result from the K-shell x-ray emission of aluminum plasmas, in the 5-8 Å (1580-2500 eV) range of the spectrum. To describe this emission we include the n=1-5 levels in Al XIII, the $1s^2$, $2s\ ^3S$,$2s\ ^1S$,$2p\ ^3P$,$2p\ ^1P$, 3-triplet, 3-singlet, n=4 and n=5 levels in Al XII, the $1s^2 2s$, 2p, 3s, 3p, 3d, n=4 and n=5 levels in Al XI, and the ground states of Al I - Al X. In addition, a number of doubly-excited levels were recently added to the model, as described in detail in the following section on satellite lines.

III. Satellite Line Model

Dielectronic satellites[4] are emission lines found in the K-shell spectrum of plasmas, lying slightly to the long-wavelength side of main resonance (Lyman) series lines of the heliumlike and hydrogenlike ions. They result from the radiative decay of doubly-excited electronic levels and potentially can be extremely useful as plasma diagnostics. In order to exploit the information contained in these lines, a detailed model has been constructed which includes several n=2 doubly-excited levels of Al XI and XII (identical models have also been built for carbon and argon), and is coupled directly to the other level structure in the CR model calculations. This level structure is shown in Fig. 1 along with the relevant transitions which give rise to the satellite lines, which lie to the low-energy side of the 1s-2p and $1s^2$-$1s2p\ ^1P$ resonance lines in the K-

shell x-ray spectrum. The scattering processes included in this model couple the doubly-excited levels to: (i) singly-excited levels of the same ion by inner-shell electron excitation and de-excitation, photo-excitation, and spontaneous and stimulated emission, (ii) the ground state of the next highest ion by electron capture and autoionization, (iii) singly-excited states of the next highest ion by electron collisional ionization and recombination, (iv) neighboring doubly-excited levels via electron impact excitation and de-excitation. Although we presently neglect ion-ion collisions between doubly-excited levels, there is reason to believe that their effect may be important for certain transitions, thus, we plan to include this process in future studies. The satellite lines, as seen in the x-ray spectrum of a typical aluminum plasma, are shown as calculated by the CR model in Fig. 2.

Although K-shell satellite line diagnostics in dense plasmas are the subject of a seperate study now in progress[5], a recently-obtained result of particular interest and significance to density determinations in dense plasmas is presented here. A well-known method of measuring ion density in hot plasmas employs the intensity ratio of the $1s^2$-$1s2p\ ^3P$ (intercombination) line to the $1s^2$-$1s2p\ ^1P$ (resonance) line in the K-spectrum[6]. As seen in Fig. 2(a), however, the s, t, m, and n satellite lines are usually unresolvably blended with the intercombination line. This poses no problem at low densities since the four satellites in question are much lower in intensity than the intercombination line. However, as the density increases, electron collisions re-distribute the doubly-excited state populations, as shown in earlier work by our group[7], resulting in a marked increase in the intensity of these satellites. As an example of this effect, we show two line ratios in Fig. 3 for a cylindrical aluminum plasma of 100 μm diameter with T_e = 600 eV at various ion densities: (1) the intercombination-to-resonance line ratio; and (2) the intercombination + s,t,m,n satellites-to-resonance line ratio. Above 10^{20} ions/cm^3 (~critical density for 1.06 μm laser light on aluminum), neglect of the four satellite lines in a theoretical modeling scheme will result in serious errors in the density determination. The effect shown is purely collisional and <u>not</u> due to opacity, since the optical depths of the satellite lines at $N_I = 4 \times 10^{21}$ ions/cm^3 is still less than 1 for a 100 μm plasma. The relative intensities of the various blended lines at this density is

0.41:0.53:0.43:0.38:1 for the IC:s:t:n:m lines. A more detailed discussion of this and other satellite line effects is being prepared for presentation under separate cover, but experimentalists using previously published results of this line ratio should exercise caution when drawing inferences from K-spectra obtained from very dense plasmas.

IV. Collisional-Radiative Non-Equilibrium Model (CRNE)

In many dense-plasma configurations, the time scale for atomic and radiative collisions is much faster than the time scale for changes in plasma parameters such as density and temperature. In these cases, collisional-radiative equilibrium (CRE) is a valid assumption, and the explicit time dependence in the atomic rate equation,

$$\frac{dN_i}{dt} = \sum_j W_{ji} N_j - \sum_j W_{ij} N_i$$

can be omitted to obtain the equilibrium solutions at any time, t, for the level populations, N_i (here, W_{ji} is a collision rate from level j to level i). If this atomic time-scale is not sufficiently fast, however, the time dependence must be retained[8] and the rate equations integrated in time as a function of the time-varying temperature, density, and size of the plasma.

Such is the case in the blowoff plasma from a CO_2-laser heated aluminum microballoon. Since the critical density for 10 μm laser light is only 10^{18} ions/cm^3 in aluminum, collisions are often not rapid enough at these (and lower) densities to equilibrate the plasma ions to rapid changes in temperature. As part of a joint program with Los Alamos National Scientific Laboratory (LANSL) to study fast-ion emission from gas-laser heated targets[9], we are attempting to characterize the ionic distributions in the plasma blowoff region using our theoretical model. As a preliminary step in this program, output from the hydrodynamic code LASNEX was provided by LANSL for post-analysis by the NRL Plasma Radiation Branch in order to calculate the relevant ion and photon emission.

Using these data, we have made comparisions between the equilibrium (CRE) and non-equilibrium (CRNE) calculations. Shown in Fig. 4 is the

calculated effective charge, Z_{eff}, for a single hydrodynamic zone in the blowoff plasma as a function of time for both CRE and CRNE assumptions. Also shown is the ion density versus time in that zone. As one can see, as the ion density drops below approximately 10^{20} ions/cm^3 for this plasma, the charge state "freezes in" while still on the ionizing part of the curve. This differs significantly from the equilibrium solution which continues to track with the rising electron temperature under the assumption that the ions respond instantaneously to the temperature changes. Similarly, as the temperature drops, the time-dependent solution shows no change in Z_{eff}, while the time-indepedent model incorrectly indicates that significant recombination is occurring. It is clear from Fig. 4 that any analysis of fast ion emission from CO_2 laser targets will require that the atomic rate-equations be integrated in time, and, thus, the CRNE model will be necessary.

V. 2-D Photon Transport Effects

A basic simplification commonly assumed in analysis of spectra from laser-produced plasma is that photon transport is treated in only one direction, along the path from the laser spot (on the target) to the spectrometer. In general, this approximation is a valid one when treating spherical target implosions. Laser interaction with flat targets, on the other hand, generates a distinctly "non-radial" plasma, and, therefore, casts doubt on the validity of 1-D codes used to model them.

In recent months, experimentalists at NRL have began using an innovative diagnostic technique called "tracer-dot implantation"[10]. Briefly, a higher-Z plug a dot of material (aluminum, for example) is implanted in a low-Z flat target (carbon). The circular plug has a diameter smaller than the laser spot-size, hence, both materials are heated and blow off from the target surface. The higher energy K-shell emission from the plug, however, will shine through the low Z target plasma relatively unattenuated and can be detected in a direction perpendicular to the target normal (or laser axis). The higher-Z plasma is collisionally contained by the low-Z blowoff and resembles a cylinder of plasma up to some distance from the target, as shown in Fig. 5(a) A slitted spectrometer can image the cylinder so that spectra can be obtained as a

function of distance from the target surface.

The preliminary theoretical analysis of these spectra has been done using the 1-D CRE model[11] by assuming that each spectrum emanates from a thin (~25-50μm) "disc" of plasma at various positions along the cylinder axis, as shown in Fig. 5(b). Under this assumption, the disc is treated as homogeneous in temperature and density, and radiation is transported along the disc radially toward the spectrometer, parallel to the foil target surface. However, this treatment neglects the photon pumping due to self-absorption along the cylinder axis (in the direction of the incoming laser beam). To perform the calculation rigorously, a 2-D radiative transfer algorithm is necessary to treat both radial and axial photon transport, and model the entire plasma cylinder self-consistently. However, we can gain some insight into the effects of axial photon pumping using our 1-D model and employing a 2-step procedure:

(1) First, we assume some typical axial temperature and density profiles, shown in Fig. 6 as solid lines, and perform a calculation in slab geometry, i.e., we transport the radiation axially. The photon pumping rates in each zone due to all surrounding zones are stored for each line and recombination edge.

(2), Then, we calculate the emission from a thin plasma disc at some distance from the target surface, say, 400 μm. The disc is assumed to be homogeneous at a temperature and density corresponding to the profiles used in step (1) at the axial position of the disc. With the CR model now in cylindrical geometry, radiation is transported radially, as was done in the earlier analyses of tracer-dots. However, the stored photon pumping rates from step (1) can be added into the rate equations to account for the axial photon pumping effects. Bear in mind that this is a time-independent analysis, hence, assumes that the plasma at a certain distance from the target surface maintains a nearly constant temperature and density during the radiation pulse time.

The calculations described above were performed for a 115 μm diameter aluminum tracer-dot implanted in a carbon target. Step (1) above was perfomed using the profiles given in Fig. 6. Then, step (2) was accomplished for five seperate plasma "discs" of thickness 50 μm, spaced evenly every 100 μm along the plasma cylinder axis. The spectra from each

of these axially pumped discs were compared with those generated from a similar disc assuming no axially pumping. As an illustration, the theoretical spectra corresponding to the disc centered at about 375 μm from the target surface (T_e=785 eV and N_I=1.7x10^{19} ions/cm^{-3}) are shown in Fig. 7(a) (no axial pumping) and Fig. 7(b) (with axial pumping). Large effects due to the axial photon pumping are seen in the Al XII and Al XIII resonance lines, while only slight differences are evident in the intercombination (IC) line, satellite (S) lines, and the higher Rydberg members of the Al XII and XIII ions. This is due to not only the large pump intensity of the resonance lines from denser plasma closer to the target but also to the larger optical depths of these lines across the thickness of the disc.

In the actual theoretical analysis of tracer-dot spectra, however, total line intensities are not used, only line ratios. Thus, we wish to quantify the errors incurred in the temperature and density determinations of the plasma by assuming isolated, radiating plasma discs and neglecting the axial pumping effects in the theoretical model. To accomplish this we analyzed the spectra generated including the axial pumping using our standard analytic techniques; the results are shown as dashed curves in Fig. 6. The density calculated from the intercombination-to-resonance line ratio is typically a factor of 2 too large, owing to the preferential axial pumping of the $1s^2$-1s2p ^1P line over the ^3P line. This reduces the line ratio which, using a plot similar to Fig. 3, yields a higher density than actually occurs, as shown by the dashed line in Fig. 6(b).

The temperature analysis, on the other hand, yielded a very interesting result. All 3 line intensity ratios used to determine temperature yielded values rather close to the actual assumed temperature profile, shown as dashed lines in Fig. 6(a) ((1) = 1s-2p/$1s^2$-1s2p ^1P, (2) = 1s-3p/$1s^2$-1s5p ^1P, (3) = 1s-2p/$1s^2$-1s3p ^1P). The reason for this apparent good agreement is in fact due to a fortuitous circumstance, since the temperature-dependent emission lines also experience significant but differing levels of axial photon pumping. However, the mis-diagnosis of the ion density due to this pumping affects the temperature determination, since the appropriate line ratio-vs-temperature curve used to get T_e will be for this incorrect density. Fortuitously, this density error somewhat

nullifies the error incurred due to the pumped temperature-sensitive lines (two "wrongs" result in a "right"), resulting in a fairly accurate determination of the actual plasma temperature. It is difficult to say, in general, whether the technique is reliable or not, based on a single diameter case with one unique set of profiles. These axial pumping effects will increase with increased dot diameter, however, and are certainly expected to exacerbate the problem of obtaining accurate values with larger implants.

One also notices the disappearance of axial photon pumping effects on the diagnostics as one approaches the target surface. This is due to two reasons: (1) as the density increases close to the target, the plasma becomes more collision-dominated, and photon pumping plays less of a role in determining the distribution of ionic level populations; (2) the main source of photons is in the dense plasma near the target surface, therefore, the flux of radiation across an areal surface is comparable in both directions, resulting in little net pumping - farther out in the blow-off, the net photon flux is almost totally away from the target, and the inclusion of optical pumping in the axial direction has a measureable effect on theoretically calculated spectra and subsequent line ratio determinations of plasma parameters.

VI. Spectral Signatures of Lateral Plasma Inhomogeneities

In this final study, our goal is to investigate the effects of lateral (perpendicular to laser beam) plasma non-uniformities on the K-shell x-ray spectrum. These non-uniformities can be the result of several phenomena, including non-uniform spatial laser intensity profile[12], varying lateral heat flow in the target[13], and fluid instabilities such as Rayleigh-Taylor[14,15]. In previous tracer-dot spectroscopy, it was assumed that that plasma density and temperature were constant in the lateral direction. Although this is probably a valid assumption for small-diameter dot implants, we questioned whether one could detect lateral inhomogeneities by increasing the diameter of the dot implant to near the scale length of the plasma inhomogeneity.

Our first step was to compare theoretical K-spectra from plasma with and without lateral inhomogeneities and look for drastic changes in the

spectral features. The plasma configuration is identical to that of the previous section and as shown in Fig. 5. The laser heats a carbon target with an aluminum tracer-dot implant smaller than the focal spot but on the order of the inhomogeneity scale length, in this case, 200 μm. A spectrometer collects aluminum K-shell radiation emitted perpendicular to the laser beam direction and is slitted to obtain data which is spatially resolved in the Z-direction (along the plasma column). Since the effects we wish to study occur predominantly in dense plasma, we concentrate on emission from a slice of the column or plasma "disc" which lies between the critical and ablation surfaces. To conduct our spectral comparison, we calculate the K-shell radiation from three hypothetical profiles for the plasma temperature and density vs. lateral position, as shown in Fig. 8, where (1) is the completely homogeneous case, (2) is a mild non-uniformity and (3) is a rather strong one. Again, we assume that these profiles are "frozen" in time during the radiation pulse and conduct a time-independent analyis.

The calculated K-spectra for the three cases considered are shown in Fig. 9. Because of the high density, the sum of the satellite line intensities appears as single features which overshadow their respective resonance lines. As the enlarged, finely-resolved spectra in Fig. 10 show, however, the resonance lines are still the single most prominent features in the spectrum. Comparing the three spectra in Fig. 9, large differences are seen in the line and continuum intensities. In the homogeneous case, the hydrogenlike Lyman lines are more intense than the heliumlike Lyman series. However, as the degree of inhomogeneity is increased, the heliumlike lines become more intense than the hydrogenlike. The reason is straightforward: the plasma non-uniformity usually results in some regions of higher temperature and lower density than the homogeneous case and other regions of higher density and lower temperature. In this temperature and density regime, the K-shell lines scale more strongly with density than temperature; hence, the denser regions found in cases (2) and (3) accentuate the colder plasma features - the heliumlike lines.

Another trend evident from Fig. 9 is the drop in Al XIV recombination edge intensity at 2.3 keV. This behavior is for the same reasons discussed above. These photons result from 2-body recombination from bare nuclei

which occur at greater abundance in the higher temperature regions of the plasma. Since the density in these regions is lower for cases (2) and (3), the intensity of this edge drops with greater inhomogeneity.

We have now seen that plasma non-uniformities between the critical and ablation surfaces can significantly alter the K-shell radiation signature. However, by using the theoretical model we have been able to generate a spectrum from both homogeneous and non-homogeneous situations with which to compare and contrast. The experimentalist, on the other hand, is not afforded the luxury of a homogeneous plasma spectrum with which he can compare his own result. How can one, therefore, conduct an experiment to determine whether non-homogeneities exist? We wish to propose a simple one which, in principle, should work.

Suppose two experiments were conducted keeping all experimental parameters identical but the tracer-dot diameter. The diameters used could be on the order of, say, 50 μm and 200 μm but both of them should be smaller than the laser focal spot-size. If the laser plasma created was in fact, free of lateral inhomogeneities, the temperature and density at some distance from the target surface should be identical for both dot diameters. Of course, this would not insure that the radiation emission perpendicular to the plasma blowoff would be identical in both cases, since the larger diameter plasma will suffer more photon re-absorption due to opacity and the line intensity ratios would change. We have compared the temperature-sensitive line ratios for both sizes of plasma at a density of 10^{21} ions/cm^3 and found that the effects of opacity would alter the ratios by only 10-20%. Moreover, one could quantitatively account for these differences using a theoretical model such as the one described here to analyze the spectra. Inhomogeneities of the magnitude shown in Fig. 8, on the other hand, should introduce large changes in the spectrum of a 200 μm tracer-dot as compared to that of a 50 μm tracer-dot, assuming the scale-length of the non-uniformity is much larger than 50 μm.

To demonstrate the feasibility of this experiment, we calculated two K-shell spectra from a tracer dot implant of only 50 μm diameter for the plasma parameters of Cases (1) and (2) in Fig. 8. The homogeneous case (Case (1)) comparison between 50 and 200 μm dots is shown in Fig. 11. Although noticeable differences are evident, they are small, particularly

between the higher Rydberg series (n>3) lines of Al XII and XIII where opacity effects are reduced as compared to the resonance lines. Shown in Fig. 12 are the theoretical K-spectra for 50 and 200 μm dots assuming the slight plasma lateral non-uniformity described by Case (2); the effect of the inhomogeneity now creates a stark contrast between the spectra. Due to the cooler, denser plasma now sampled by the larger diameter implant, heliumlike features are far more intense than hydrogenlike features, including both line and continuum. Although an experiment of this sort will not verify the physical phenomena responsible for the inhomogeneity, it is an obvious indicator of its existence. In addition, the diameter of the dot implant can be systematically varied to assess the approximate scale length of the non-uniformity. With detailed theoretical modeling of the spectrum, the probable temperature and density profile could even be predicted, shedding light on the most likely cause of the inhomogeneity, be it Rayleigh-Taylor instabilities, extreme lateral heat transport, or non-uniform laser profile, Of course, this experiment depends on the fact that the temperatures in the region of interest are high enough to have sufficient K radiation for detection. At lower temperatures (T_e < 150 eV), lithiumlike or beryllium emission lines may have to be used to detect inhomogeneities. Fluid code calculations, however, predict that significant K-shell emission is usually generated behind the critical surface and that it is intense enough for easy detection.

VII. Conclusions

Although the studies discussed in this work are preliminary in nature, several conclusive statements can be made regarding these results. First, early investigation with a new atomic model designed to treat doubly-excited levels and satellite line emission has revealed that the plasma density diagnostic involving the $1s^2$-$1s2p\ ^3P$/$1s^2$-$1s2p\ ^1P$ line intensity ratio can yield spurious results at high densities. This is due to the effects of unresolvable satellite lines blended with the intercombination line. Second, we have reaffirmed the result obtained by other authors that the low density blow-off region of laser-produced plasmas are highly non-equilibrium in nature. In order to describe the ionization and radiation dynamics in these regions, the explicit time-dependence of the level population rate equations should be included and the rate equations

integrated in time as a function of the changing plasma density, temperature, and size.

Third, we have substantiated the need for two-dimensional radiation transport modeling for tracer-dot spectroscopy by including the effects of axial photon pumping in a laser-produced plasma in a "post-analysis" way while treating lateral radiation transfer in a self-consistent manner. The effect on density determinations is seen to be about a factor of two in the region in front of the critical surface, while the temperature determination gave a fortuitously accurate result. It will be the subject of a more in-depth study to determine whether this is the case, in general, or whether it is a result particular to the size and temperature parameters chosen for this work.

Finally, we have investigated the effects of lateral inhomogeneities (due to laser beam non-uniformity or plasma effects) on the K-shell spectrum and found them to be significant for the conditions studied. Typically, the plasma regions of higher density are weighted more heavily in the spectral signature. In an effort to inform the experimentalist of the existence of such plasma inhomogeneities, we have shown that a simple experiment involving different tracer-dot diameters should give conclusive evidence. We have demonstrated that the effects of increased path length (due to larger "dot" diameters) on the photon re-absorption should have a relatively small impact on the relative intensities of features in the K-shell spectrum as compared to the effects of lateral inhomogeneities; thus, these non-uniformities should be straightforward to detect using this scheme.

We would like to thank J. Rogerson and M. Blaha for their assistance with the satellite line model, J. Apruzese for valuable discussions regarding radiative transfer, and F. Begay and R. Goldman of Los Alamos for supplying us with the hydro code output. We would also like to express our thanks to M. J. Herbst and R. R. Whitlock for introducing the technique of spot-spectroscopy to us.

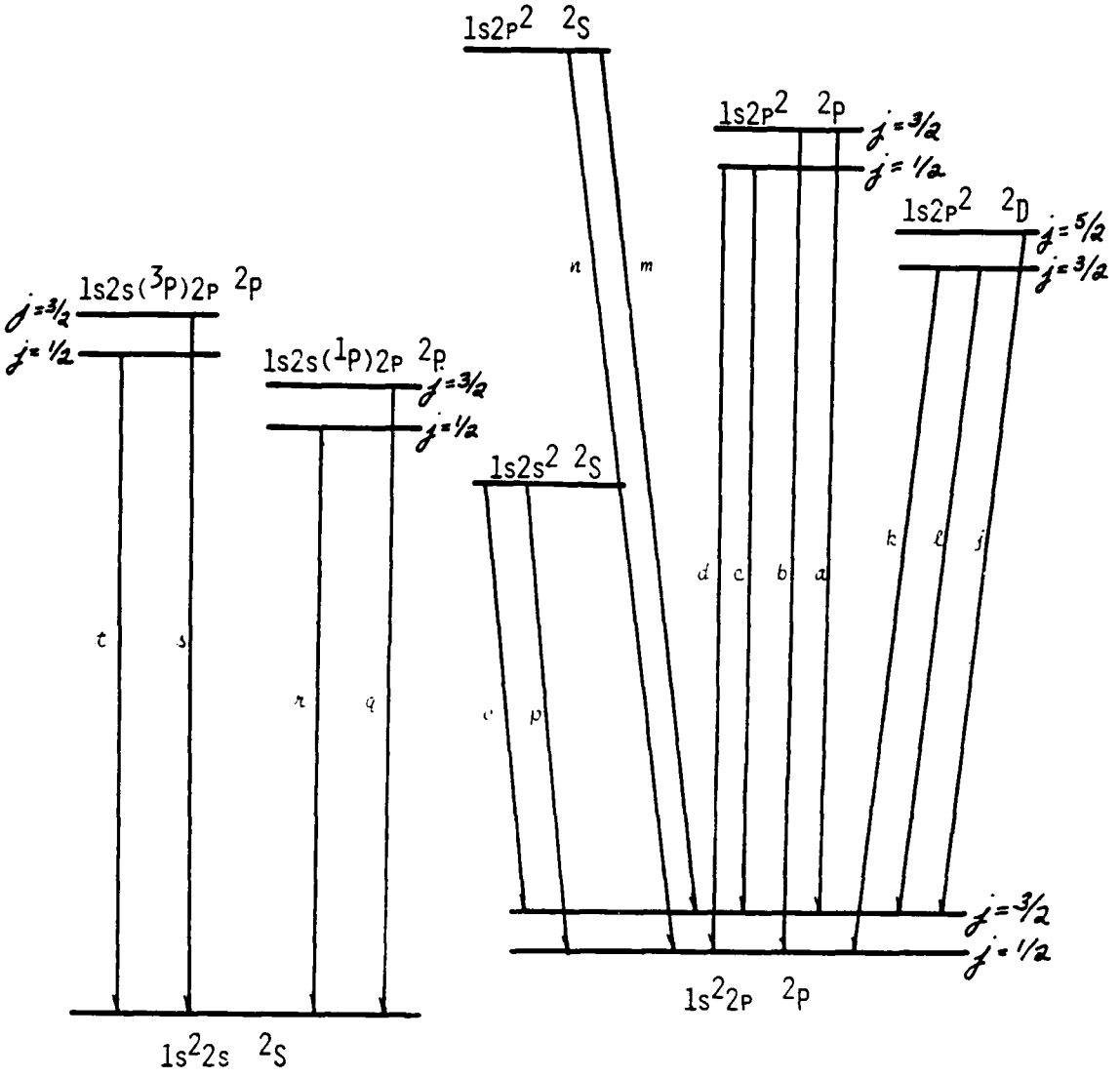

Fig. 1(a) — Doubly-excited level structure and satellite lines for the lithiumlike ion.

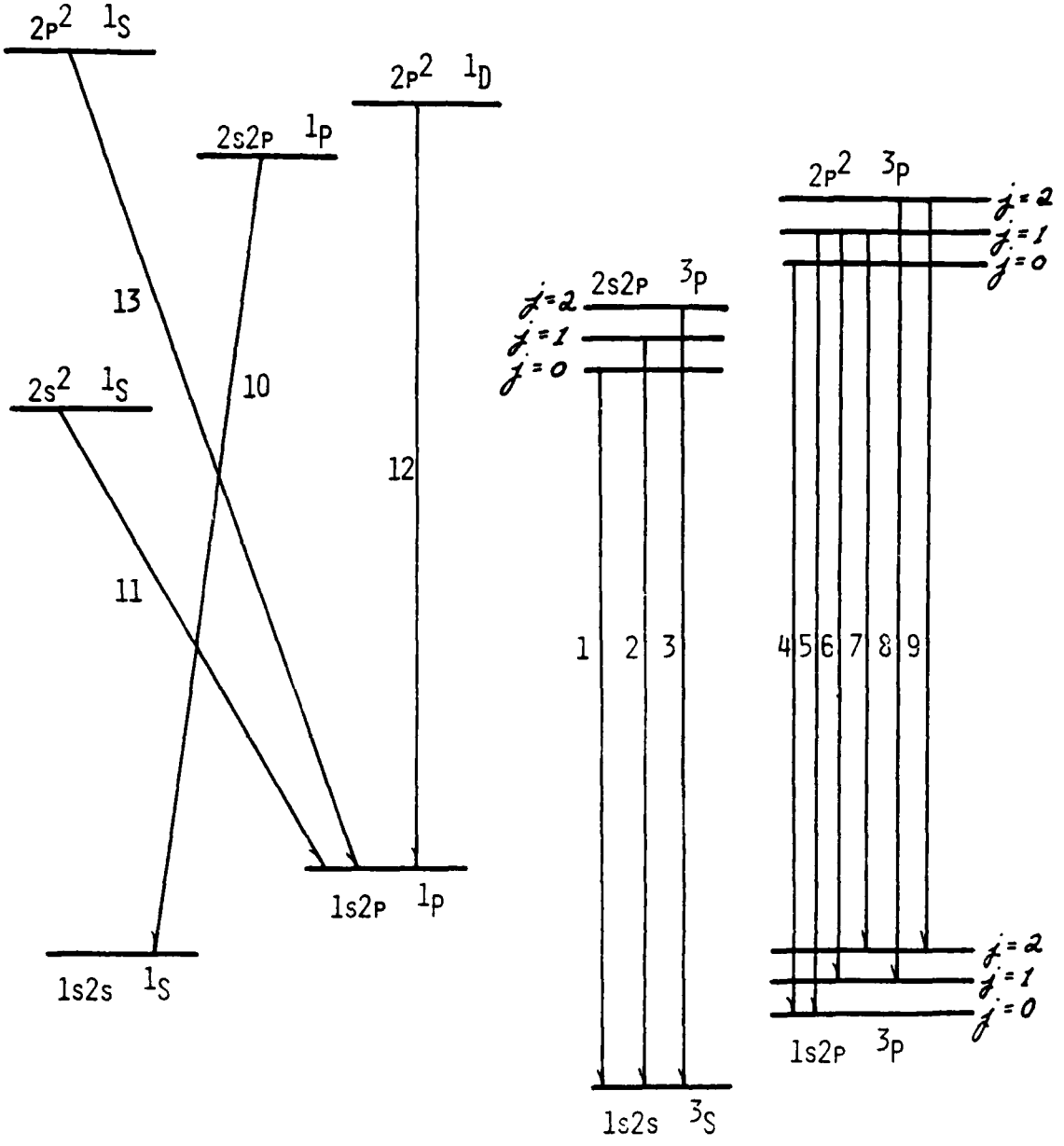

Fig. 1(b) — Doubly-excited level structure and satellite lines for the heliumlike ion.

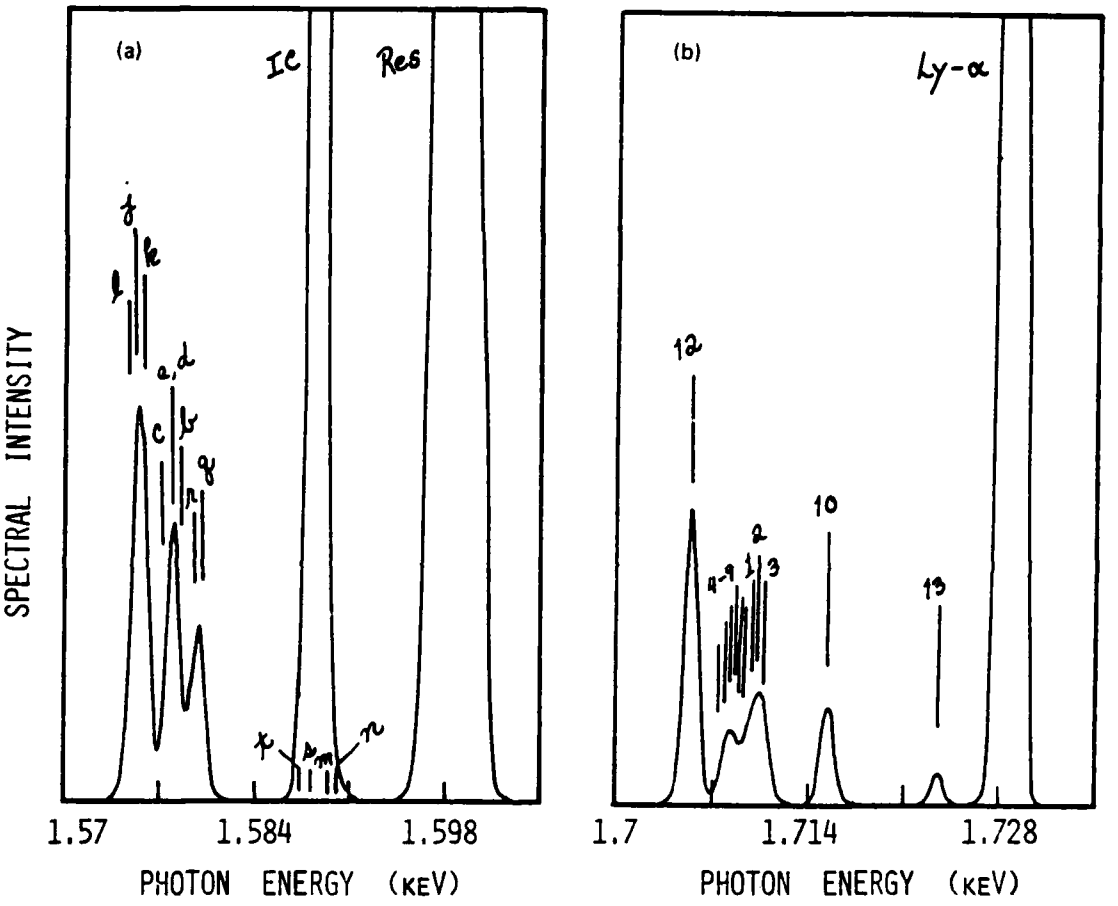

(a) — Typical lithiumlike satellite spectrum

(b) — Typical heliumlike satellite spectrum

Figure 2

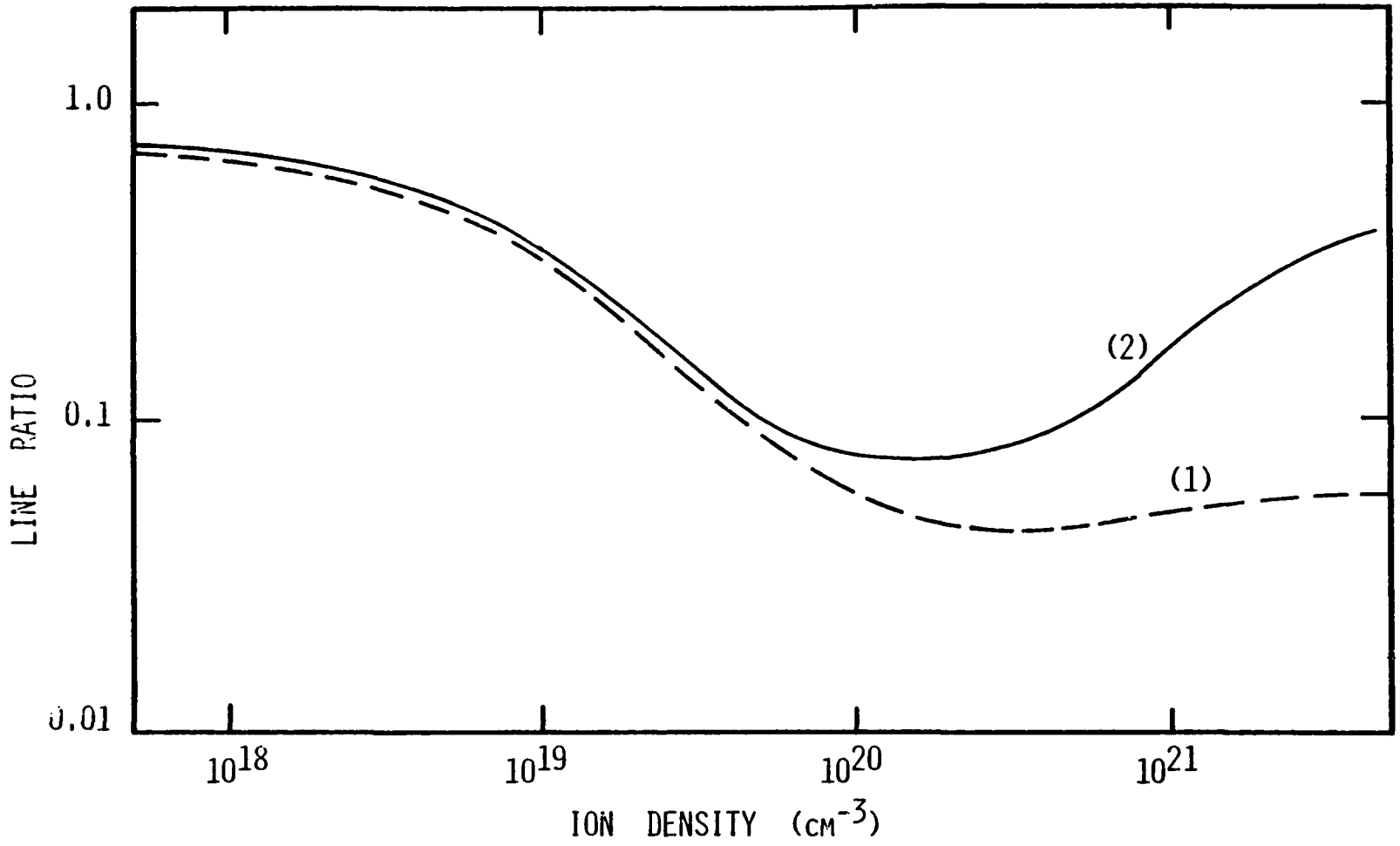

Fig. 3 — Heliumlike line ratios vs. ion density for a 100 μm diameter aluminum plasma cylinder at 600 eV. The solid line is the (s,t,n,m + IC)/Resonance line ratio; the dashed line is just the IC($1s^2$-$1s2p\ ^3P$)/Resonance ($1s^2$-$1s2p\ ^1P$) line ratio.

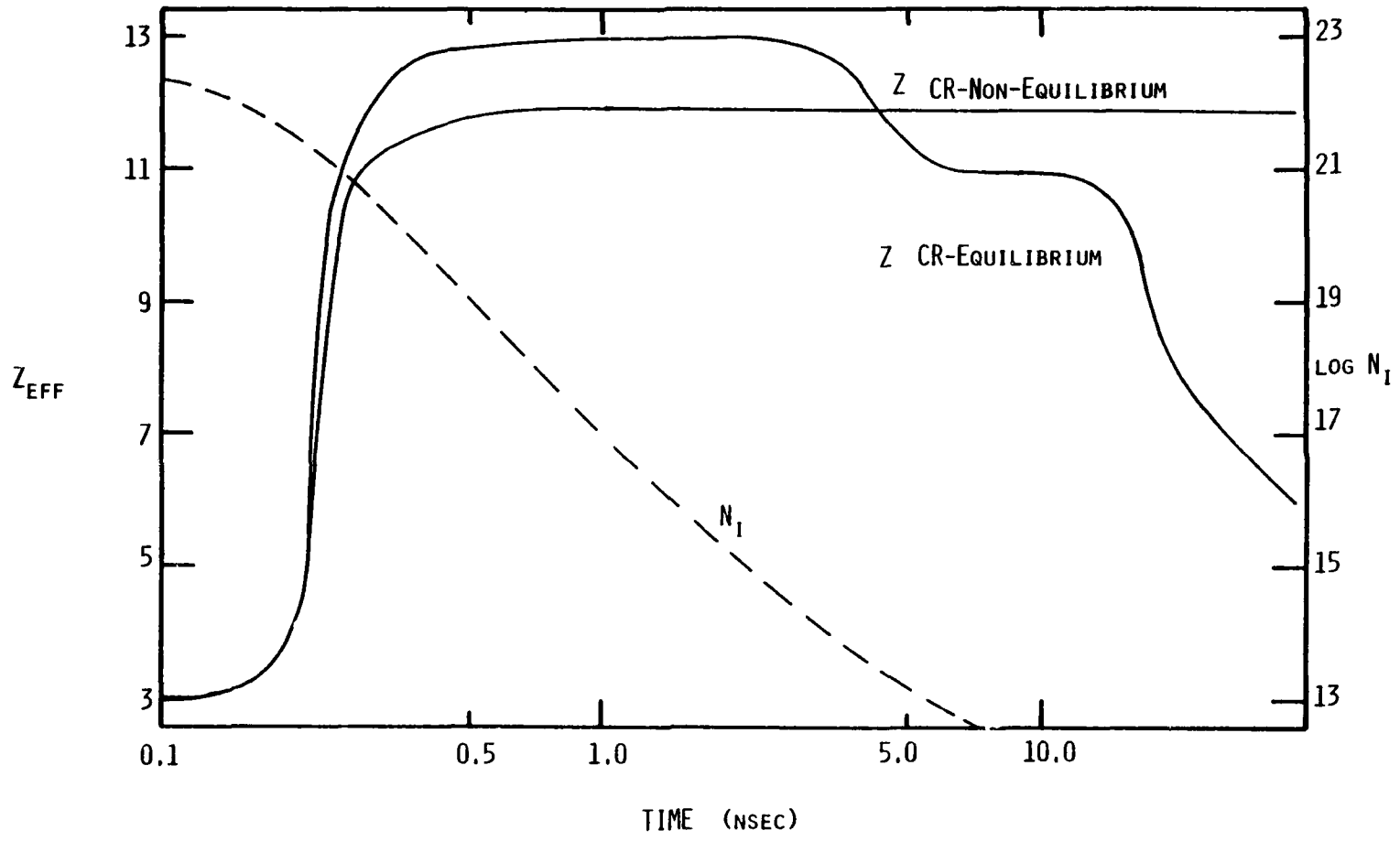

Fig. 4 — The Z_{eff} and ion density vs. time for a zone in the blowoff of a CO_2-laser-heated aluminum microballoon, as calculated by the CRE and CRNE ionization models (post-analysis of LASNEX hydro-code plasma profiles).

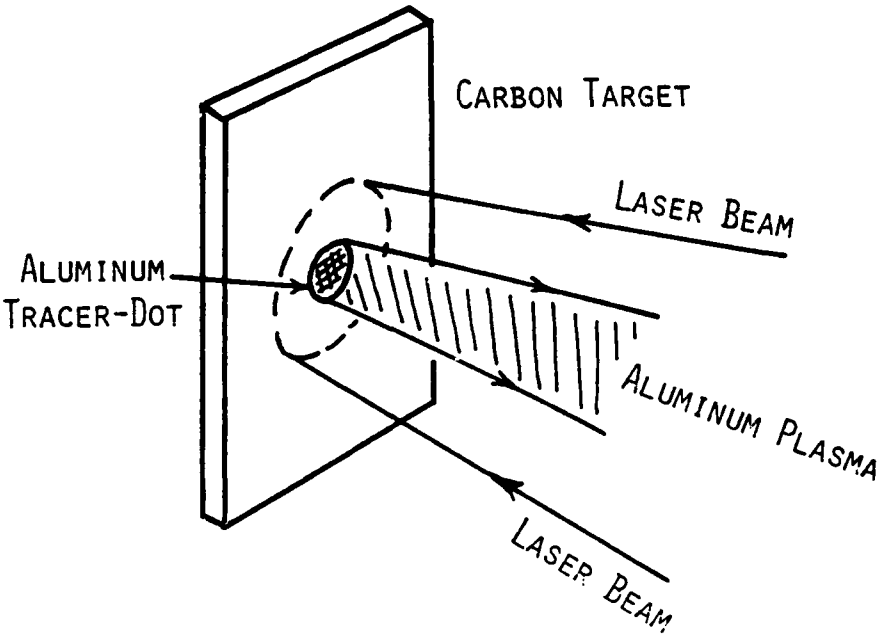

(a) — Sketch of laser beam-tracer-dot target interaction

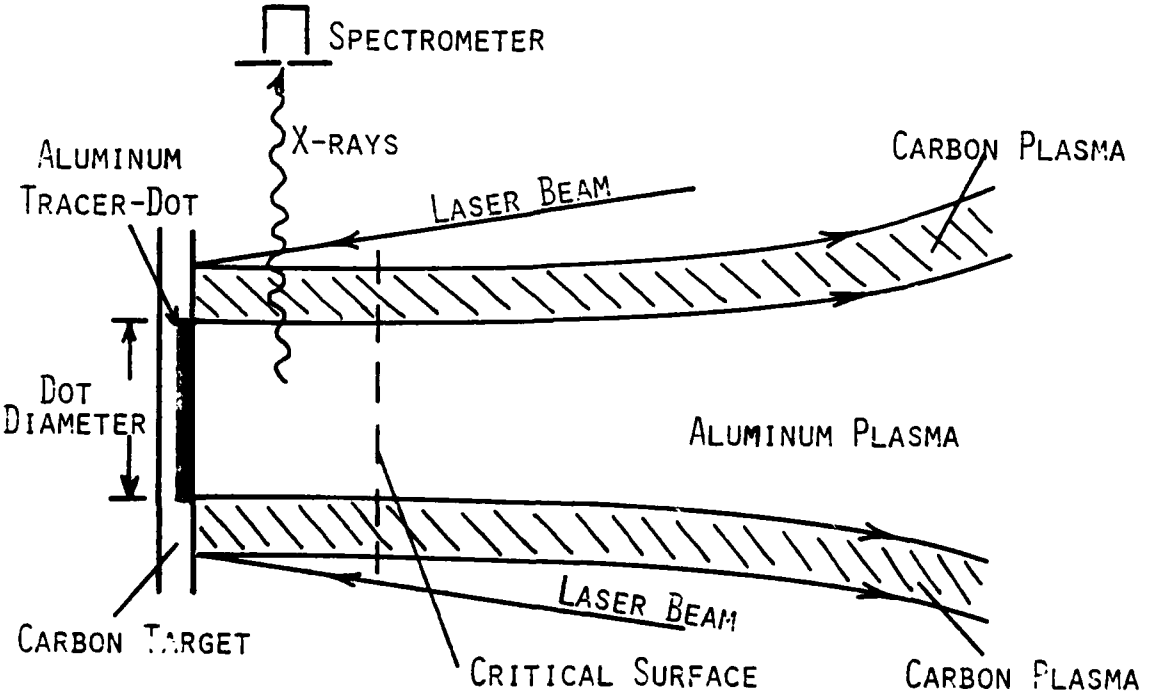

(b) Schematic for tracer-dot spectroscopy of a laser-heated target

Figure 5

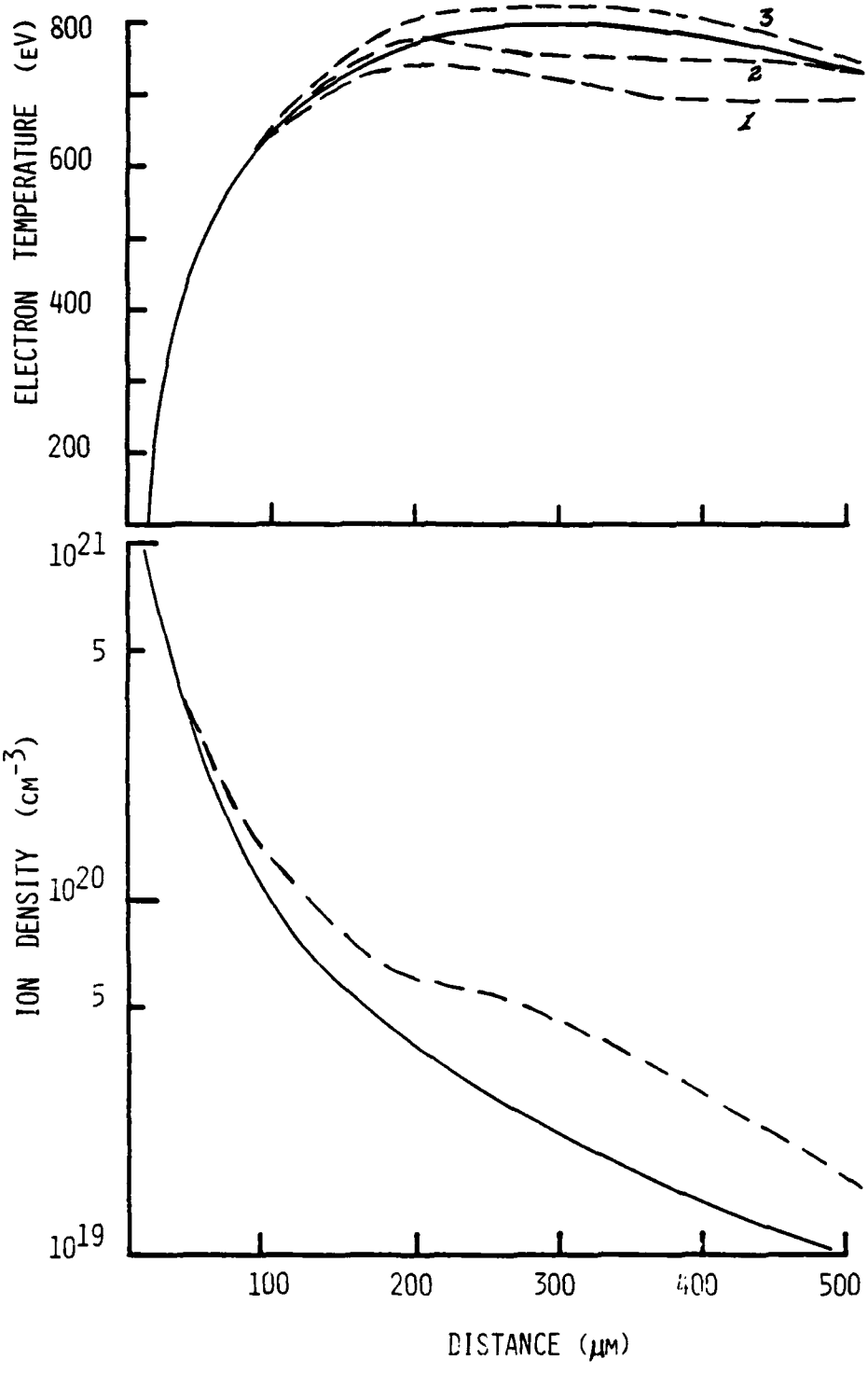

Fig. 6 — Axial (normal to target) plasma temperature and density profiles assumed for the axial photon pumping effects investigation.

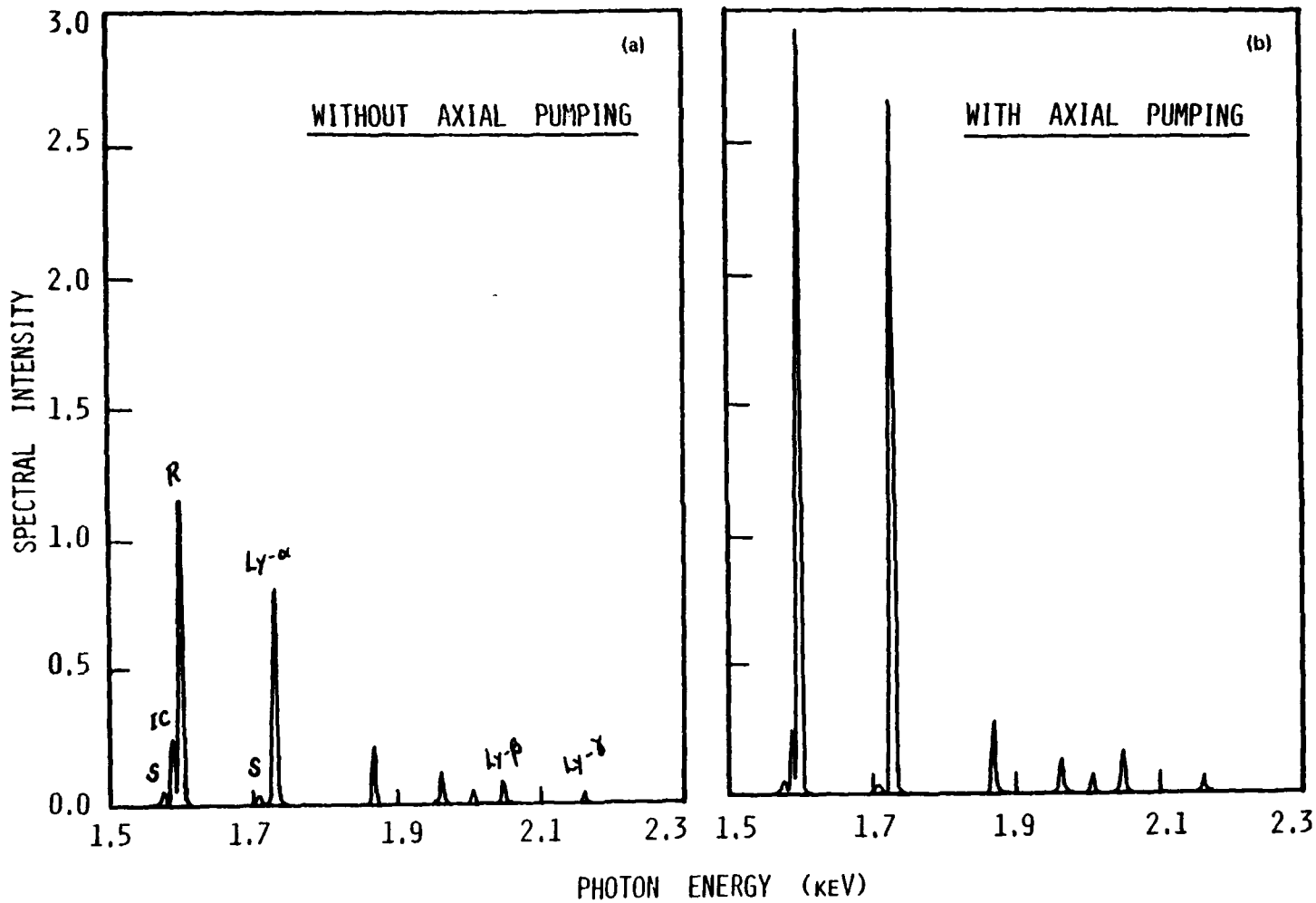

(a) — K-shell X-ray spectrum without accounting for axial photon pumping

(b) — K-shell X-ray spectrum accounting for axial photon pumping

Figure 7

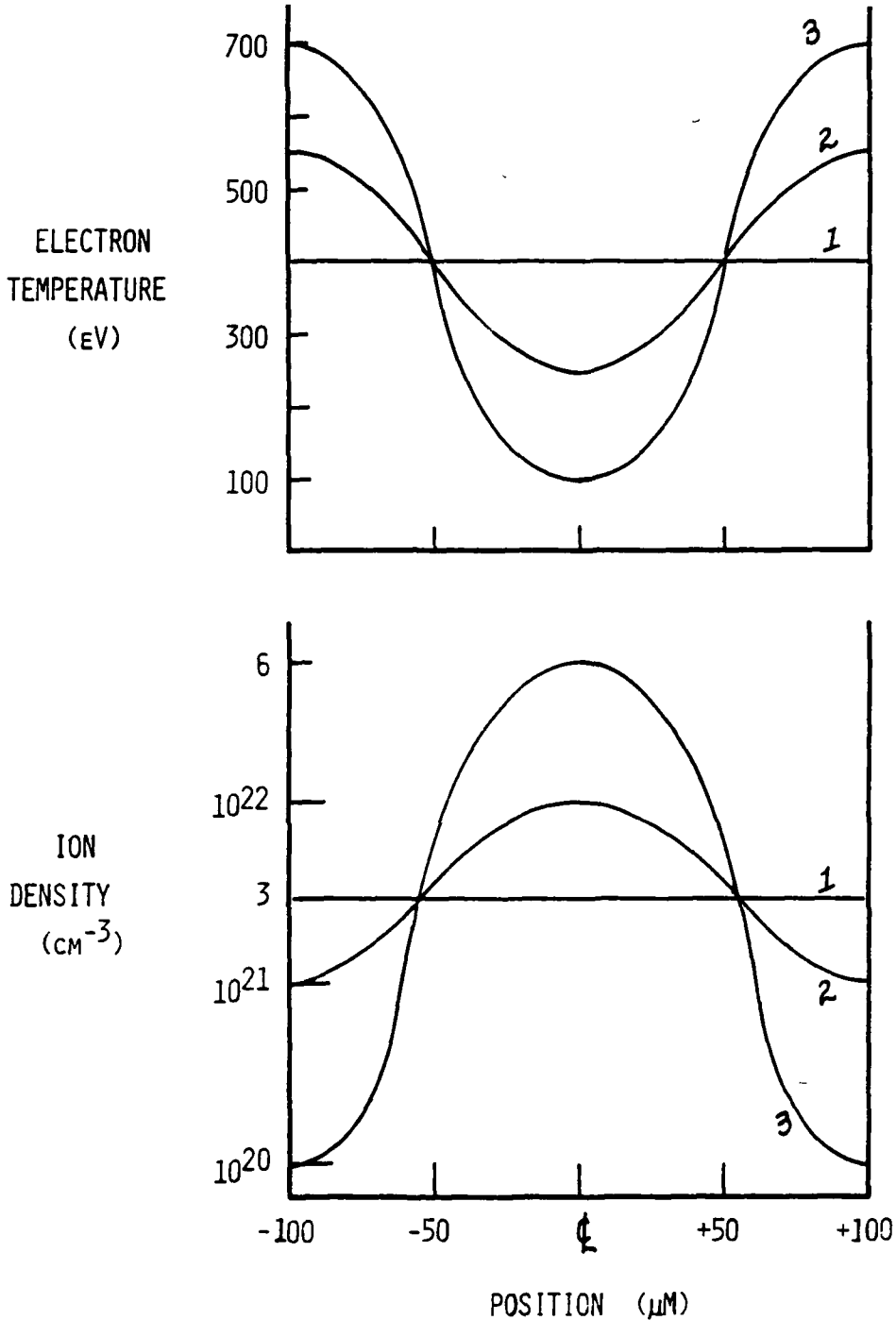

Fig 8 — Lateral (parallel to target) plasma temperature and density profiles assumed in the lateral plasma non-uniformity effects investigation.

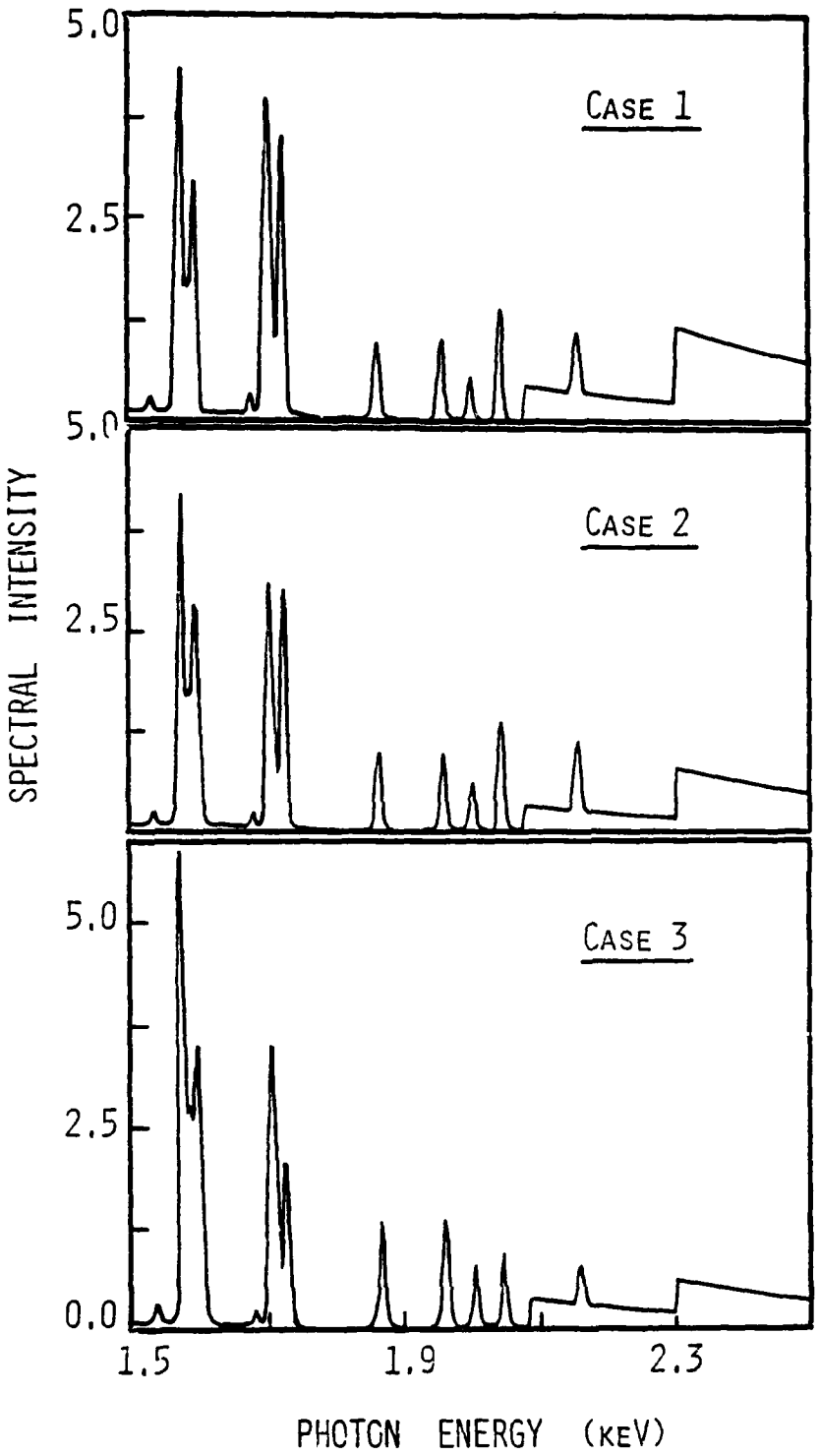

Fig. 9 — The K-shell X-ray spectra for a 200 μm diameter aluminum tracer dot corresponding to the 3 plasma profiles shown in Fig. 8.

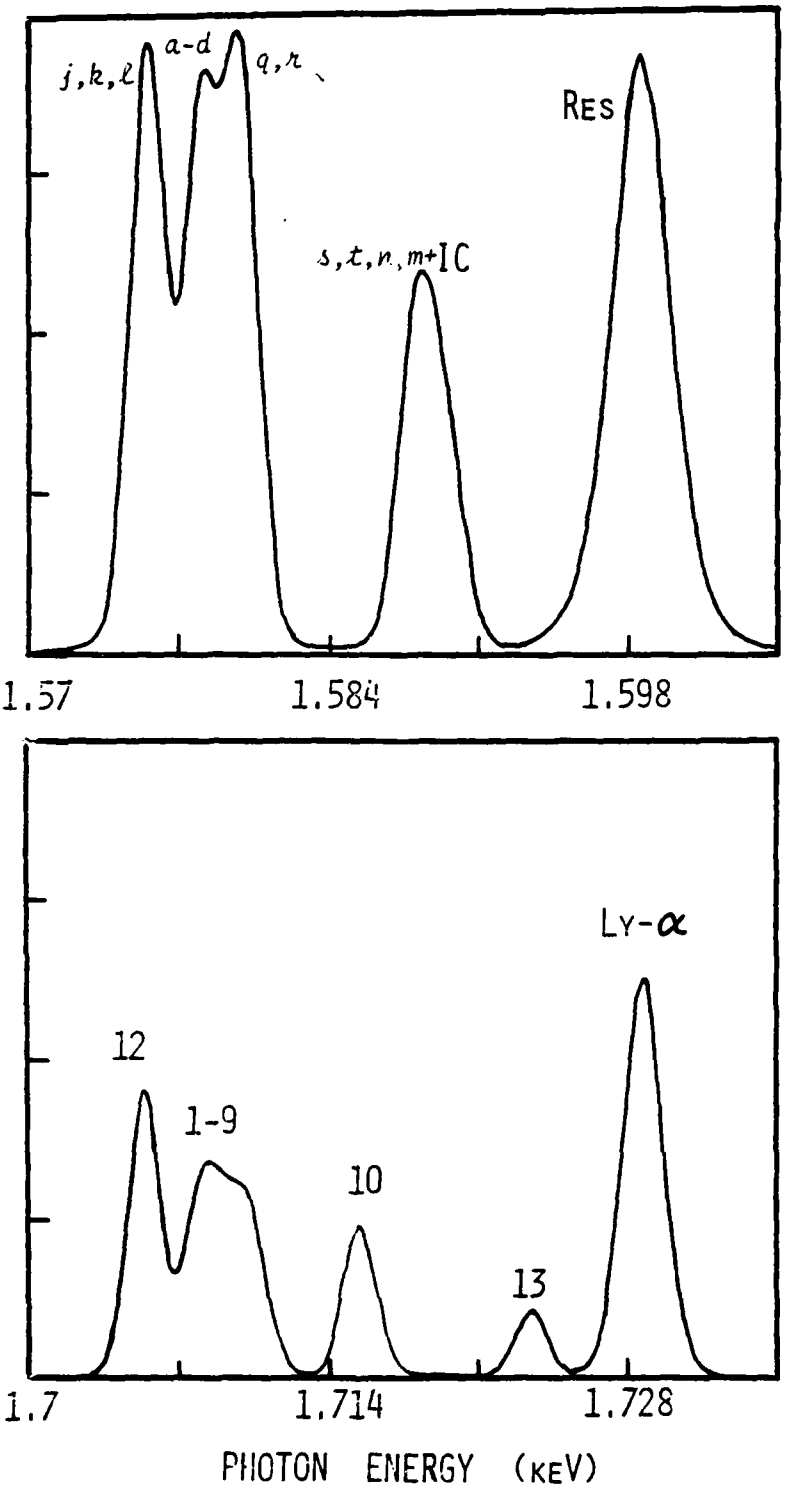

Fig. 10 — A blow-up of the resonance and satellite line regions of the K-shell spectrum for Case 1 in Fig. 13, showing the spectral features with greater resolution.

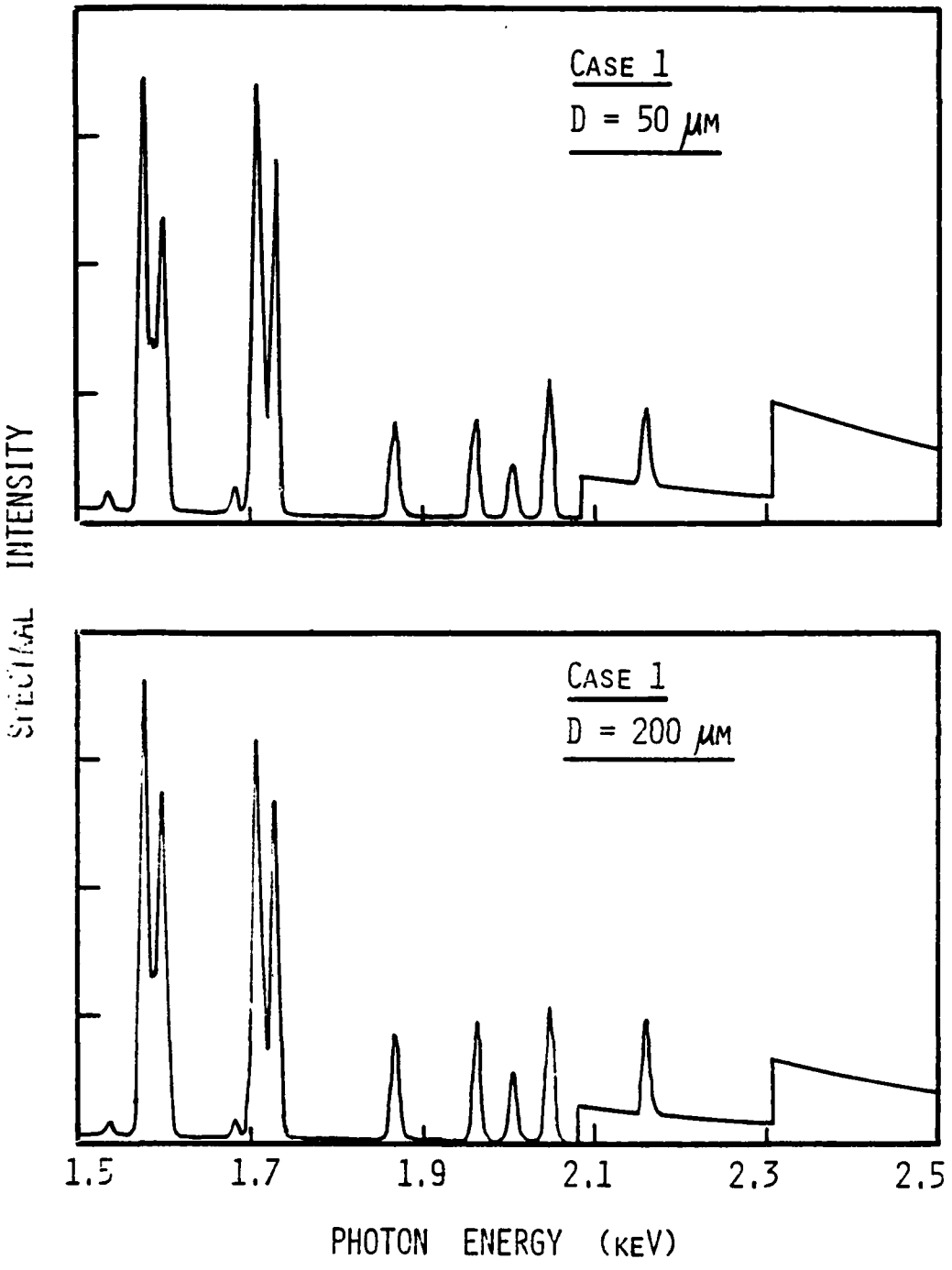

Fig. 11 — The K-shell X-ray spectra for Case 1 in Fig. 8, comparing 50 μm and 200 μm diameter tracer-dots.

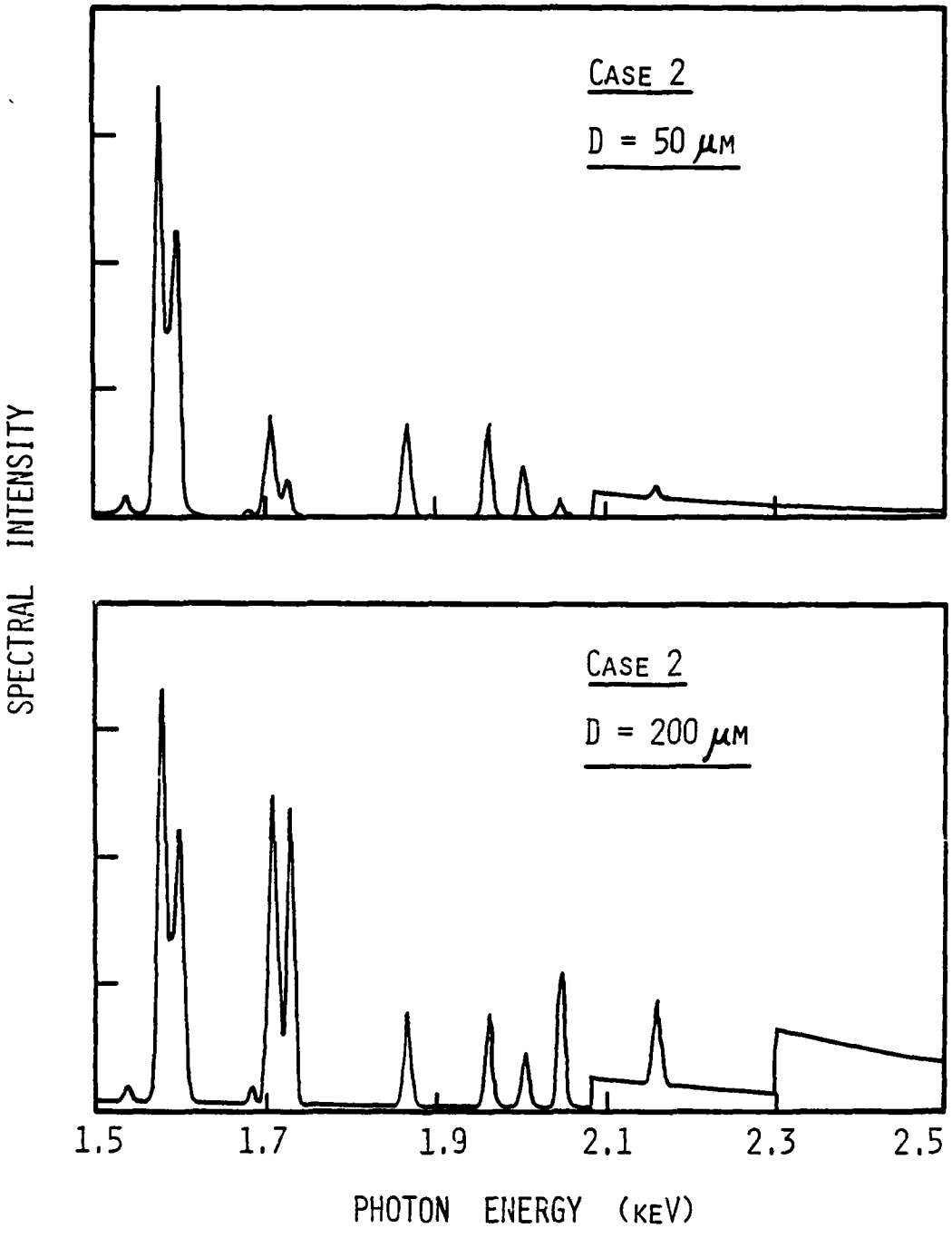

Fig. 12 — The K-shell X-ray spectra for Case 2 in Fig. 8, comparing 50 μm and 200 μm diameter tracer-dots.

References

1. D. Duston and J. Davis, Bull. APS 27, No. 8, 1082 (Oct. 1982).
2. J. P Apruzese, J. Davis, D. Duston, and K. G. Whitney, JQSRT 23, 479 (1980).
3. D. Duston and J. Davis, Phys. Rev. A 21, 1664 (1980); _____ Phys. Rev. A 23, 2602 (1981); _____ Phys. Rev. A 24, 1505 (1981); _____ JQSRT 27, 267 (1982).
4. A. H. Gabriel and Carole Jordan, in Case Studies in Atomic Collision Physics, ed. by E. W. McDaniel and M. R. McDowell (North-Holland, Amsterdam, 1972) Vol. 2.
5. D. Duston, J. Davis, J. E. Rogerson and M. Blaha (to be published).
6. A. V. Vinogradov, I. Yu. Skobelev and E. A. Yukov, Kvant. Elektron. (Moscow) 2, 1165 (1975) [Sov. J. Quantum Electron. 5, 630 (1975)].
7. V. L. Jacobs and M. Blaha, Phys. Rev. A 21, 525 (1980).
8. M. Mattioli, Plasma Physics 13, 19 (1971) and M. K. Matzen and J. S. Pearlman, Phys. Fluids 22, 449 (1979).
9. F. Begay and D. W. Forslund, Phys. Fluids 25, 1675 (1982).
10. M. J. Herbst and J. Grun, Phys. Fluids 24, 1917 (1981) and M. J. Herbst, P. G. Burkhalter, J. Grun, R. R. Whitlock, and M. Fink, Rev. Sci. Instr. 53, 1418 (1982).
11. M. J. Herbst et al., to appear in Laser Interaction and Related Plasma Phenomena, V. 6, ed. by H. Hora.
12. M. H. Emery, J. H. Orens, J. H. Gardner and J. P. Boris, Phys. Rev. Lett. 48, 253 (1982).
13. D. W. Forslund and J. U. Brackbill, Phys. Rev. Lett. 48, 1614 (1982).
14. M. H. Emery, J. H. Gardner and J. P. Boris, Phys. Rev. Lett. 48, 677 (1982).
15. C. P. Verdon et al., Phys. Fluids 25, 1653 (1982).

DISTRIBUTION LIST

Assistant to the Secretary of Defense Atomic Energy Washington, D.C. 20301 ATTN: Executive Assistant	1 Copy
Defense Technical Information Center Cameron Station 5010 Duke Street Alexandria, VA 22314	2 copies
Director Defense Intelligence Agency Washington, D.C. 20301 ATTN: DT-1B R. Rubenstein	1 Copy
Director Defense Nuclear Agency Washington, D.C. 20305	
ATTN: DDST	1 copy
ATTN: TITL	4 copies
ATTN: RAEV	1 copy
ATTN: STVI	1 copy
Commander Field Command Defense Nuclear Agency Kirtland AFB, New Mexico 87115 ATTN: FCPR	1 Copy
Chief Field Command Livermore Division Department of Defense P.O. Box 808 Livermore, CA 94550 ATTN: FCPRL	1 Copy
Director Joint Strat TGT Planning Staff Offutt AFB Omaha, Nebraska 68113 ATTN: JSAS	1 Copy

Undersecretary of Defense
for RSCH and ENGRG
Department of Defense
Washington, D.C. 20301
ATTN: Strategic and Space Systems (OS)

1 Copy

Deputy Chief of Staff for RSCH DEV and ACQ
Department of the Army
Washington, D.C. 20301
ATTN: DAMA-CSS-N

1 Copy

Commander
Harry Diamond Laboratories
Department of the Army
2800 Powder Mill Road
Adelphi, MD 20783
ATTN: DELHD-N-NP
ATTN: DELHD-R J. Rosado
ATTN: DELHD-TA-L (Tech. Lib.)

1 copy each

U.S. Army Missile Command
Redstone Scientific Information Center
Attn: DRSMI-RPRD (Documents)
Redstone Arsenal, Alabama 35809

3 Copies

Commander
U.S. Army Missile Command
Redstone Arsenal, Alabama 35898
ATTN: DRCPM-PE-EA

1 copy

Commander
U.S. Army Nuclear and Chemical Agency
7500 Backlick Road
Building 2073
Springfield, VA 22150
ATTN: Library

1 copy

Commander
U.S. Army Test and Evaluation Command
Aberdeen Proving Ground, MD 21005
ATTN: DRSTE-EL

1 Copy

Commanding Officer
Naval Intelligence Support Center
4301 Suitland Road, Bldg. 5
Washington, D.C. 20390
ATTN: NISC-45

1 Copy

Commander — 1 Copy
Naval Weapons Center
China Lake, CA 93555
ATTN: Code 233 (Tech. Lib.)

Office of the Chief of Naval Operations — 1 Copy
Washington, D.C. 20350
ATTN: R. Blaise

Officer in Charge — 1 copy each
White Oak Laboratory
Naval Surface Weapons Center
Silver Spring, MD 20910
ATTN: Code R40
ATTN: Code F31

Air Force Weapons Laboratory — 1 copy each
Kirtland AFB, New Mexico 87117
ATTN: SUL
ATTN: CA
ATTN: APL
ATTN: CA

Deputy Chief of Staff
Research, Development and Accounting — 1 Copy
Department of the Air Force
Washington, D.C. 20330
ATTN: AFRDQSM

Space and Missile Systems Organization/IN — 1 Copy
Air Force Systems Command
P. O. Box 92960
Worldway Postal Center
Los Angeles, CA 90009
ATTN: IND D. Muskin (Intelligence)

HQ BMO/MM — 1 Copy
Norton AFB, CA 92409
ATTN: Col. J. M. Wells

Space and Missile Systems Organization/SK — 1 Copy
Air Force Systems Command
Post Office Box 92960
Worldway Postal Center
Los Angeles, CA 90009
ATTN: SKF P. Stadler (Space Comm. Systems)

AVCO Research and Systems Group — 1 Copy
201 Lowell Street
Wilminton, MA 01887
ATTN: Library A830

BDM Corporation — 1 Copy
7915 Jones Branch Drive
McLean, Virginia 22101
ATTN: Corporate Library

Boeing Company — 1 Copy
P. O. Box 3707
Seattle, WA 98134
ATTN: Aerospace Library

The Dikewood Corporation — 1 Copy
1613 University Bldv., N.E.
Albuquerque, New Mexico 8710
ATTN: L. Wayne Davis

EG and G Washington Analytical — 1 Copy
Services Center, Inc.
P. O. Box 10218
Albuquerque, New Mexico 87114
ATTN: Library

General Electric Company — 1 Copy
Space Division
Valley Forge Space Center
P. O. Box 8555
Philadelphia, PA 19101
ATTN: J. Peden

General Electric Company - Tempo — 1 Copy
Center for Advanced Studies
816 State Street
P.O. Drawer QQ
Santa Barbara, CA 93102
ATTN: DASIAC

Institute for Defense Analyses — 1 Copy
1801 N. Beauregard St.
Alexandria, VA 22311
ATTN: Classified Library

IRT Corporation — 1 Copy
P.O. Box 81087
San Diego, CA 92138
ATTN: R. Mertz

JAYCOR — 1 Copy
11011 Forreyane Rd.
P.O. Box 85154
San Diego, CA 92138
ATTN: E. Wenaas

JAYCOR — 1 Copy
205 S. Whiting Street, Suite 500
Alexandria, VA 22304
ATTN: R. Sullivan

KAMAN Sciences Corp. — 1 copy each
P. O. Box 7463
Colorado Springs, CO 80933
ATTN: J. Hoffman
ATTN: A. Bridges
ATTN: D. Bryce
ATTN: W. Ware

Lawrence Livermore National Laboratory — 1 copy each
University of California
P.O. Box 808
Livermore, California 94550
Attn: DOC CDN for L-153
Attn: DOC CDN for L-47 L. Wouters
Attn: DOC CDN for Tech. Infor. Dept. Lib.

Lockheed Missiles and Space Co., Inc. — 1 copy each
P. O. Box 504
Sunnyvale, CA 94086
Attn: S. Taimlty
Attn: J.D. Weisner

Lockheed Missiles and Space Co., Inc. — 1 Copy
3251 Hanover Street
Palo Alto, CA 94304
Attn: L. Chase

Maxwell Laboratory, Inc. — 1 Copy each
9244 Balboa Avenue
San Diego, CA 92123
ATTN: A. Kolb
ATTN: W. Clark
ATTN: D. Tanimoto

McDonnell Douglas Corp. — 1 Copy
5301 Bolsa Avenue
Huntington Beach, CA 92647
ATTN: S. Schneider

Mission Research Corp. — 1 Copy each
P. O. Drawer 719
Santa Barbara, CA 93102
ATTN: C. Longmire
ATTN: W. Hart

Mission Research Corp.-San Diego — 1 Copy
5434 Ruffin Rd.
San Diego, California 92123
ATTN: Victor J. Van Lint

Northrop Corporation — 1 Copy
Northrop Research and Technology Center
1 Research Park
Palos Verdes Peninsula, CA 90274
ATTN: Library

Northrop Corporation — 1 Copy
Electronic Division
2301 120th Street
Hawthorne, CA 90250
ATTN: V. Damarting

Physics International Company — 1 Copy each
2700 Merced Street
San Leandro, CA 94577
Attm: C. Stallings
Attn: B. Bernstein
Attn: E. Goldman

R and D Associates — 1 Copy each
P.O. Box 9695
Marina Del Rey, CA 90291
ATTN: W. Graham, Jr.
ATTN: P. Haas

Sandia National Laboratories — 1 Copy Each
P.O. Box 5800
Albuquerque, New Mexico 87115
ATTN: Doc Con For 3141

Science Applications, Inc. — 1 copy
P. O. Box 2351
La Jolla, CA 92038
ATTN: J. Beyster

Spire Corporation — 1 copy
P. O. Box D
Bedford, MA 01730
ATTN: R. Little

SRI International — 1 copy
333 Ravenswood Avenue
Menlo Park, CA 94025
ATTN: S. Dairiki

Sytems, Science and Software, Inc. — 1 copy
P. O. Box 1620
La Jolla, CA 92038
ATTN: A. Wilson

Texas Tech University — 1 copy
P.O. Box 5404
North College Station
Lubbock, TX 79417
ATTN: T. Simpson

TRW Defense and Space Systems Group — 1 Copy
One Space Park
Redondo Beach, CA 90278
ATTN: Technical Information Center

Vought Corporation — 1 Copy
Michigan Division
38111 Van Dyke Road
Sterling Heights, Maine 48077
ATTN: Technical Information Center
(Formerly LTV Aerospace Corp.)

Naval Research Laboratory
Plasma Radiation Group
Washington, D.C. 20375

Code 4720	-	150 Copies
Code 4700	-	26 Copies
Code 2628	-	20 Copies